

SHORT THESIS FOR THE DEGREE OF DOCTOR OF PHILOSOPHY (PHD)

Characterization of the role of poly(ADP-ribose) polymerases in psoriasis

by Dóra Antal

Supervisor: Dr. Magdolna Szántó



UNIVERSITY OF DEBRECEN
DOCTORAL SCHOOL OF MOLECULAR MEDICINE

DEBRECEN, 2023

Characterization of the role of poly(ADP-ribose) polymerase enzymes in psoriasis

By Dóra Antal, Expert in Public Health, MSc

Supervisor: Magdolna Szántó, PhD

Doctoral School of Molecular Medicine, University of Debrecen

Head of the Defense Committee: János Szöllősi, PhD, DSc, MHAS

Reviewers: Anikó Miskeiné Kapitány, PhD
Roberta Fajka-Boja, PhD

Members of the Defense Committee: Katalin Erdélyi, PhD

Ferenc Fenyvesi, PhD

The PhD Defense takes place at the Lecture Hall of Building A, Department of Internal Medicine, Faculty of Medicine, University of Debrecen, at 1 PM, 15th of November, 2023.

Introduction

The connection between PARP enzymes and inflammation

The post-translational modification of proteins catalyzed by members of the poly(ADP-ribose) polymerase (PARP) enzyme family, known as ADP-ribosylation, was originally detected during the repair of DNA breaks. However, research over the last decades has shed light on numerous physiological processes where PARPs play significant roles. These include processes such as transcription, translation, cell differentiation, cell death, and the regulation of cellular metabolism.

PARP activity within cells is largely covered by PARP1 (85-90%) and PARP2 (5-15%) activity. Despite their structural and functional similarities, these two enzymes have distinct biological roles. PARP activation and ADP-ribosylation have been described in various inflammatory processes. In mice, the deletion of PARP1 resulted in reduced inflammation in T helper 2 (Th2) type inflammatory models, such as asthma, allergic airway inflammation, acute pancreatitis, colitis, and contact hypersensitivity mouse models. Limited information is available regarding the role of PARP2 in inflammation, but based on current knowledge, it seems that PARP2 may not have a known role in Th2-type inflammations. However, a general observation is that inhibiting PARP activity using pan-PARP inhibitors, which target not only PARP1 but also PARP2 and even PARP3, leads to anti-inflammatory effects not only in animal models but also in humans.

Psoriasis

Psoriasis is a chronic, immune-mediated, inflammatory skin disease characterized by hyperproliferation and abnormal differentiation of epidermal keratinocytes. The pathogenesis of psoriasis is a complex process, with activated T cells, especially Th1 and Th17 types, likely being the primary modulators responsible for initiating and sustaining inflammation. However, psoriasis cannot be solely explained by T-cell activation, and other non-classical immune cells, such as epidermal keratinocytes, likely play a significant role in the expression of the disease. The specific cause of psoriasis development is still unclear, resulting in the absence of a definitive cure. Currently, the most effective approach in psoriasis therapy targets cytokines produced by T cells using biological agents, which has marked a significant breakthrough in treating the disease. Nevertheless, biological therapy comes with numerous side effects,

prompting the need for novel solutions in psoriasis treatment. The emergence of mouse models for psoriasis has contributed to expanding our understanding of the disease's pathomechanism and facilitating the development of more effective therapies.

Poly(ADP-ribose) (PAR) has been detected in normal skin keratinocytes, hair follicle cells, endothelial cells, sebaceous gland cells, subcutaneous adipocytes, indicating that PAR might regulate physiological functions in these cell types. Activation of PARP1 has been described in various skin pathophysiological conditions, such as sunburn, melanoma, and contact hypersensitivity. However, less is known about the potential role of PARP2 in the skin. Unlike PARP1, PARP2 does not participate in contact hypersensitivity reactions, suggesting a different role for PARP2 in skin pathophysiology. Since the roles of PARPs in Th1 and Th17 type inflammatory processes are less understood, the goal of my PhD work is to characterize the roles of both PARP1 and PARP2 in psoriasis.

Aims

In our work, we aimed to uncover the potential roles of PARP1 and PARP2 in regulating inflammation characteristic of psoriasis and to address the question of whether dysregulation of PARP1 and/or PARP2 might be involved in the pathomechanism of psoriasis.

Several literature data suggest that PARP1 may primarily play a role in the development of Th2-type inflammation, as the deletion of PARP1 resulted in decreased inflammation in various Th2-type inflammatory mouse models. In contrast, we have fewer data on the role of PARP2 in inflammation. However, based on existing knowledge, we assumed that the roles of PARP1 and PARP2 could differ in the regulation of inflammation, as the role of PARP2 is not known in Th2-type inflammatory processes.

In the first part of our work, our co-authors examined the imiquimod-induced psoriasis model in PARP1^{-/-} mice, where contrary to literature data, they identified PARP1 as an anti-inflammatory factor and observed exacerbation of symptoms. Based on these findings, for our further investigations, we set the following objectives:

1. Investigation of PARP1 expression in skin biopsies of psoriasis patients.
2. Study of the reaction of keratinocytes to imiquimod treatment and PARP inhibition in *in vitro* cell culture experiments.

Given the effects observed in the psoriasis model investigation for PARP1, we wanted to explore whether PARP2 could also play a role in the development of psoriasis. To address this, in the second part of our work, we formulated the following objectives:

1. Examination of PARP2 expression in skin biopsies of psoriasis patients.
2. Study of the psoriasis mouse model, imiquimod-induced skin inflammation, in PARP2^{-/-} mice.
3. Investigation of the molecular mechanisms underlying the phenotype in PARP2^{-/-} mice in *in vitro* cell culture experiments using PARP2 silenced keratinocytes.

Material and methods

Cell culture

The cellular studies were conducted using a human immortalized keratinocyte cell line (HPV-Ker) established by the Creative Laboratory team in Szeged. To create this cell line, normal human epidermal keratinocytes (NHEK) were obtained from a healthy individual's sample during routine plastic surgery. Subsequently, the cells were transfected with a cucumber mosaic virus vector (pCMV) containing the human papillomavirus (HPV) E6/16 oncogene. Through 70 passages of continuous cultivation, the stable cell line was established.

The HPV-Ker cells were cultured in keratinocyte serum-free medium (SFM), supplemented with bovine pituitary extract (BPE) (50 µg/ml), human recombinant epidermal growth factor (rEGF) (5 ng/ml), 1% penicillin/streptomycin, and 1% L-glutamine solution.

PARP2-silenced HPV-Ker keratinocytes (shPARP2) and negative control keratinocytes (scPARP2) were maintained in the same composition of keratinocyte-SFM medium as described above, supplemented with an additional 2.5 µg/ml puromycin dihydrochloride to sustain the selection of transfected cells.

The cells were maintained under standard laboratory conditions in a cell culture incubator at 37 °C with an atmosphere of 5% (v/v) carbon dioxide.

shRNA-mediated gene silencing

To establish PARP2 gene-silenced HPV-Ker keratinocytes (shPARP2), we utilized pre-designed short hairpin RNA (shRNA) sequences targeting PARP2, which were cloned into the pLKO.1 vector and packaged into lentiviral particles. Negative control HPV-Ker cells (scPARP2) were created through transduction with lentiviral particles containing a non-targeting shRNA sequence. The pLKO.1 vector also conveyed puromycin resistance gene, enabling selection of puromycin-resistant cells with 2.5 µg/ml puromycin dihydrochloride following transduction.

To assess the success of silencing and monitor its persistence throughout our further experiments, both mRNA and protein levels of silenced genes were periodically examined. Western blot and RT-qPCR methods were employed for this purpose.

Differentiation of HPV-Ker cells

To induce differentiation of HPV-Ker scPARP2 and shPARP2 keratinocytes, the cells were either seeded into 6-well culture plates (6×10^5 cells/well) or placed in Petri dishes (22.1 cm², 1.4×10^6 cells/dish). After three days or four days in the case of Petri dishes, one day after the cell culture reached full confluence, the medium was replaced, and the differentiation of cells was initiated using keratinocyte serum-free medium supplemented with human rEGF (5 ng/ml), BPE (50 µg/ml), and 1.7 mM Ca²⁺. After three days, the differentiation process was stopped. IL17A (200 ng/ml) and TNF α (10 ng/ml) treatments were applied in the differentiating medium.

Analysis of total protein quantity changes in HPV-Ker cells

To assess the proliferation of HPV-Ker keratinocytes, we utilized the sulforhodamine B (SRB) assay, which measures changes in total protein content within the cells, correlating with their proliferation. Cells were seeded into 96-well plates (2×10^4 cells/well), followed by treatment with imiquimod (100 µM) and PARP inhibitors (OLA-1 µM, PJ34-3 µM, or RUCA-1 µM) or treatment with imiquimod alone without inhibitors for a duration of 3 hours. At the end of the treatment, cells were fixed with 50% trichloroacetic acid (TCA) and incubated at 4°C for 1 hour. After washing the cells, they were stained with SRB solution (0.4% (w/v) in 1% acetic acid). Unbound dye was removed by washing with 1% acetic acid. The bound dye was dissolved in 10 mM Tris base. Absorbance was measured at 540 nm using a spectrophotometer.

Cell cycle analysis of keratinocytes

HPV-Ker sc and shPARP2 cells were seeded into Petri dishes (TPP, 60.1 cm², 9×10^5 cells/petri), and after 24 hours, IL17A + TNF α treatment was applied to the cells for 6 hours. After the treatment, cells were washed with PBS, detached from the bottom of the Petri dishes using trypsin, followed by another PBS wash. The cells were then centrifuged at 10,000 x g for 5 minutes. Subsequently, cells were fixed dropwise with 5 ml of ice-cold 70% ethanol while slowly vortexing, then incubated overnight at 4 °C. The next day, cells were centrifuged at 10,000 x g for 10 minutes for 5 minutes. Cells were resuspended in 1% BSA-PBS buffer, washed, and then 100 µg/ml propidium iodide stock solution was added to the buffer (1 µl/sample), and the mixture was incubated in the dark for 20 minutes. Cell cycle analysis was conducted using the NovoCyte flow cytometer.

NF-κB activity assay

HPV-Ker sc and shPARP2 cells were seeded into 6-well culture plates (TPP, 1.5X10⁵ cells/well), followed by pre-treatment with exemestane (5 μM-24h). Subsequently, IL17A+TNFα combined treatment was applied to the cells for 6 hours. Proteins were extracted from the cells using Complete Lysis Buffer AM2, and the protein content in the supernatant was determined using the Pierce BCA protein assay kit. The activation of the NF-κB p65 subunit was assessed in 4 μg of total cell protein extract from each sample using the TransAM™ NFκB p65 Chemi Kits according to the manufacturer's instructions. For positive control of NFκB p65 activation, phorbol myristate acetate (PMA) and calcium ionophore-treated Jurkat nuclear extract provided in the kit were used. Luminescence was measured using a Spark 10M microplate reader.

Determination of cellular cytokine and estradiol concentrations

Supernatants from HPV-Ker sc and shPARP2 cells exposed to different treatments were collected, and the concentrations of IL6, IL23A, IL17C, and estradiol in the supernatants were determined using commercially available ELISA kits. All materials used for ELISA were provided by the kits, and every step was strictly followed according to the manufacturer's instructions. Due to variations in protocols described by different manufacturers, a general overview of the ELISA measurement process is presented.

ELISA microplates included in the kits were pre-coated with specific antibodies. Pre-prepared standards and samples were pipetted into appropriate wells and incubated for varying durations. In some kits, this step was preceded by incubation with a primary antibody. This was followed by incubation with different cytokine or estradiol conjugates and then multiple washes. Hydrogen peroxide and a chromogenic substrate, tetramethylbenzidine, in equal proportion, were added to each well, initiating a color reaction. The color reaction was halted by adding sulfuric acid, and absorbance was immediately read at the specified wavelength using a spectrophotometer. The quantity of cytokines and estradiol was determined in pg/ml or ng/L using a standard curve. IL23A and IL17C were not detectable in the supernatant, therefore, this will not be presented.

Immunocytochemistry

HPV-Ker sc and shPARP2 cells were grown on circular glass coverslips (4×10^4 cells/coverslip) in 24-well culture dishes and added IL17A+TNF α after 48h estradiol (1nM) pretreatment. At the end of treatment, cells were gently washed with PBS and fixed in ice-cold methanol at -20 °C for 10 min. After fixation, cells were washed three times with PBS, followed by permeabilization with 1% Triton X-100 - PBS solution for 10 minutes. The cells were blocked with a 1% BSA solution dissolved in PBS for 1 hour at room temperature, and then incubated with the primary antibody overnight at 4 °C. On the next day, cells were washed three times with PBS and incubated with a fluorophore-labeled secondary antibody for 1 hour. Cell nuclei were visualized with DAPI staining for 10 minutes. The coverslips were mounted on microscope slides using a Mowiol/Dabco solution (49:1). For image acquisition, a Leica TCS SP8 confocal microscope was used, and the images were captured using the LAS AFv3.1.3 software.

RNA Isolation and RT-qPCR

The cells were plated in 6-well plates (TPP, 2.5×10^5 cells/well), and total RNA was isolated from the cells using TRIzol reagent following the manufacturer's instructions. For RNA sequencing, RNA samples were isolated using the Qiagen RNeasy Kit as per the manufacturer's instructions. The concentration and purity of RNA were assessed using a NanoDrop ND-1000 spectrophotometer, followed by treatment with Ambion DNase I to remove any unwanted DNA from the samples. Subsequently, 1 µg of RNA sample was used for reverse transcription with the High-Capacity cDNA Reverse Transcription Kit.

The RT-qPCR reactions were performed using fluorescently labeled single-stranded oligonucleotides, known as TaqMan probes, and the TaqMan Gene Expression Master Mix protocol on a LightCycler 480 Real-Time PCR instrument. Glyceraldehyde-3-phosphate dehydrogenase (GAPDH) was used as an internal control.

RNA sequencing (RNA-Seq)

In order to obtain complete transcriptome data, high-throughput mRNA sequencing analysis was performed on Illumina sequencing platform. The quality of total RNA samples was assessed using Agilent BioAnalyzer with the Eukaryotic Total RNA Nano Kit following the manufacturer's protocol. Samples with an RNA Integrity Number (RIN) value greater than

7 were selected for library preparation. RNA-Seq libraries were prepared from total RNA using the Ultra II RNA Sample Prep kit following the manufacturer's protocol. Briefly, poly-A RNAs were captured using oligo-dT-conjugated magnetic beads, followed by washing and fragmentation at 94 degrees Celsius. First-strand cDNA was generated through random priming reverse transcription, followed by second-strand synthesis to generate double-stranded cDNA. After end repair, adapter ligation, and enrichment PCR to amplify adapter-ligated fragments, sequencing libraries were created. Sequencing was performed on an Illumina NextSeq 500 instrument using 75-cycle single-end sequencing. For data analysis, raw sequencing data (fastq) were aligned to the GRCh38 human reference genome version using the HISAT2 algorithm to create BAM files. Downstream analysis was conducted using the StrandNGS software (www.strand/ngs.com). BAM files were imported into the DESeq software, and the DESeq algorithm was used for normalization. Moderated t-tests with Benjamini-Hochberg FDR correction were employed to identify genes expressed under different conditions. The CytoScape v3.4 software with the ClueGo v2.3.5 application was used to identify overrepresented Gene Ontology (GO) terms. Using a list of differentially expressed genes and the GO biological process database, a two-sided hypergeometric test was performed with Bonferroni correction. The RNA sequencing data is available in the BioProject database: <https://www.ncbi.nlm.nih.gov/bioproject/PRJNA889321>.

Protein extraction

HPV-Ker cells were cultured in Petri dishes (TPP, 22.1 cm², 2×10⁶ cells/dish). At the end of the treatments, cells were washed with PBS and collected in lysis buffer (50 mM Tris, 150 mM NaCl, 1% Triton X-100, 0.5% sodium deoxycholate, 0.1% SDS, 1 mM EDTA, 1 mM Na₃VO₄, 1 mM NaF, 1 mM PMSF, protease inhibitor cocktail) kept on ice. DNA-protein complexes in cell lysates were resolved by sonication at 15 s intervals with 3×20 pulses. Protein isolates were separated from debris by centrifugation at 10,000 × g for 10 minutes at 4 °C. Protein concentration was determined using the Pierce BCA protein assay kit.

Cell fractionation

For separation of cytosolic and nuclear protein fractions, HPV-Ker cells were washed with ice-cold PBS, collected, and centrifuged at 3000 × g for 10 minutes at 4 °C. Pellets were homogenized in 600 µl Buffer A (10 mM HEPES - pH 7.9; 10 mM KCl, 1 mM EDTA, 1 mM EGTA, 1 mM DTT, protease inhibitors, and 0.5% Nonidet-P), and lysed using a 1 ml syringe

with a 26-G needle. Lysates were vortexed, and intact nuclei were confirmed by trypan blue staining. Subsequently, lysates were centrifuged at 15,000 x g for 1 minute at 4°C, and the resulting supernatant was used as the cytosolic fraction. Pellets were washed with 400 µl Buffer A, followed by further lysis using a needle. Then, pellets were centrifuged at 15,000 x g for 1 minute at 4 °C in Buffer B (20 mM HEPES - pH 7.9; 420 mM NaCl, 0.5 mM EDTA, 0.5 mM EGTA, 1 mM DTT, protease inhibitors). After sonication on ice (3x20 pulses, 15-second intervals), pellets were centrifuged at 12,000 x g for 10 minutes at 4 °C to obtain the nuclear fraction. Protein concentration was determined using the Pierce BCA protein assay kit.

Western Blot

Protein lysates were boiled in 5x SDS sample buffer (310 mM Tris-HCl, pH 6.8, 50% glycerol, 10% SDS, 100 mM DTT, 0.01% bromophenol blue), supplemented with 2-mercaptoethanol, for 10 minutes at 100°C. Protein extracts (25-35µg) were separated on 8-10% polyacrylamide gels and transferred onto nitrocellulose membranes. Membranes were blocked with 5% BSA-TBS_{Tween} or 5% non-fat dry milk-TBS_{Tween} solution for 1 hour at room temperature, followed by overnight incubation with primary antibodies at 4 °C. The next day, membranes were incubated with peroxidase-conjugated secondary antibodies specific to the primary antibodies for 1 hour at room temperature. Signals were visualized using enhanced chemiluminescence and captured with a ChemiDocTM Touch system. Band intensities were quantified using Image lab 5.2.1 software.

Animal experiments

Mice

The animal experiments were performed under a licence registered by the University of Debrecen's Working Animal Experimentation Committee (DEMÁB) (registration number: 15/2016/DEMÁB), in compliance with the relevant laws, government regulations and European Union directives.

For our experiments, we used PARP2^{+/+} and PARP2^{-/-} mice with a C57BL/6J genetic background obtained through heterozygous crosses. The breeding and housing of mice were carried out at the Animal Facility of the Institute of Biochemistry and Molecular Biology, Life Science Building, University of Debrecen (registration number: III/4-KÁT/2015). Each cage housed up to six mice, which were housed in standard block-sized cages (365 × 207 × 140 mm, 530 cm² surface area; Eurostandard II type L, supplied by Techniplast) and lined with Lignocel

Select Fine bedding. Environmental enrichment was provided to mice through paper rolls. Dark-light cycles were controlled on a 12-12-hour basis, and the temperature was maintained at a constant 22 ± 1 °C. Animals had access to food and sterilized tap water ad libitum. Cages were changed weekly on the same day, and the animal facility was under veterinary supervision. Animal breeding took place in a Specific Pathogen-Free (SPF) certified facility. For our experiments, only male mice aged 8-16 weeks were selected, and during the experiments, mice were housed individually.

The psoriasis mouse model - IMQ-induced dermatitis

To establish the IMQ model, mice were first divided into treatment groups ($\text{PARP2}^{+/+}$ CTL n=6 IMQ n=8 EXE+IMQ n=8; $\text{PARP2}^{-/-}$ CTL n=5 IMQ n=7 EXE+IMQ n=7). A 2×2 cm area of hair was removed from the back of male mice using depilatory cream, taking care to avoid skin damage. Subsequently, the mice were treated daily with 62.5 mg of 5% imiquimod-containing Aldara cream or vehicle cream for 4 days to induce psoriasis-like lesions. To inhibit aromatase, a solution of exemestane dissolved in 500 µM dimethyl sulfoxide (DMSO) was applied to the hairless skin of the mice 30 minutes before Aldara treatment, once daily. The severity of lesions, including skin thickening, erythema, and scaling, was evaluated daily by two experienced independent dermatologists using a scale ranging from 0 to 4, where 0 indicated no symptoms and 4 represented the most severe symptoms. On the 5th day, 2 hours before sacrifice, mice received intraperitoneal injections of BrdU solution (100 mg/kg body weight). After sacrifice, the affected skin areas were excised for further histological examination.

Cytokine profiling in mouse skin

Mouse skin samples were immediately placed in liquid nitrogen after excision and stored at -80 °C until the start of our investigations. Prior to protein extraction, the tissues were rinsed with PBS and their mass was measured. The tissues were homogenized in PBS containing 10X protease inhibitor cocktail using 5 mm stainless steel beads, at a frequency of 30 hertz for 8 minutes using a TissueLyser II. Subsequently, Triton X-100 was added to the samples to reach a final concentration of 1%. The samples were then centrifuged at $10000 \times g$ for 5 minutes at 4 °C to remove the remaining skin tissues. The supernatant was collected, and the protein content was measured using the Pierce BCA protein assay kit. Within each treatment group, individual samples were pooled to obtain a total of 300 µg of protein per group. The

cytokine profiling of mouse was determined using a kit so-called cytokine array, following the protocol provided by the manufacturer. The pre-manufactured nitrocellulose membranes contained spotted antibodies, enabling the determination of multiple cytokines and chemokines simultaneously.

The immunoblot images were captured and visualized using the ChemiDoc Touch Imaging System. Image analysis was conducted with the CellProfiler 3.1.5 software. The spots on the retrieved membrane images were covered using a template provided in the kit, which included the specific arrangement of the spots. Circles symbolizing the positions of the immobilized antibodies were manually adjusted to maximize alignment with the spots. The blank, white areas of the membrane were segmented, and areas were selected according to the size threshold of the circles symbolizing the positions of the immobilized antibodies. The raw spots were expanded by 3 pixels to remove irregularities at the edges and then shrunk to their central pixels. The refined spots were generated by expanding the central pixel until they covered the original cytokine spots on the membrane. Cytokine signals on the original images were measured within the circular areas of the refined dots.

Further cytokine determination by ELISA in mouse skin

Protein samples obtained from tissue homogenates of mice were used to detect TNF α , IL17A and IL17C cytokines using commercially available ELISA kits. Prepackaged ELISA microplates were coated with mouse TNF α , IL17A or IL17C specific antibodies. Standard and sample dilutions were prepared in sample dilution buffer. For mouse IL17A and mouse TNF α , samples were diluted by $\frac{1}{2}$ -fold, while for mouse IL17C, samples were diluted threefold to prevent matrix components from affecting the results. Standards and samples were added to the appropriate wells and incubated at 37 °C for 90 minutes. After 90 minutes, the plates were washed twice with wash buffer, and then a solution containing biotinylated antibodies was added to each well, followed by incubation at 37 °C for 1 hour. Subsequently, the plates were washed three times. After washing, a solution containing peroxidase-conjugated streptavidin was added to each well, and the plates were incubated at 37 °C for 30 minutes. A mixture of H₂O₂ and tetramethylbenzidine in equal proportions was added to each well, resulting in a color reaction. The color reaction was stopped by adding sulfuric acid, and the absorbance was immediately measured at 450 nm using a spectrophotometer. The quantity of cytokines was determined in pg/ml based on the standard curve.

Immunohistochemistry

Immunohistochemistry analyses were performed on 4 µm thick sections cut from formalin fixed, paraffin embedded mouse or human skin samples. Heat-induced antigen retrieval was performed on formalin-fixed samples. EDTA buffer was applied in a microwave oven for 15 minutes to expose the epitopes of the target proteins. Endogenous peroxidase activity was blocked with 3% H₂O₂ for 10 minutes. After blocking, tissue sections were incubated with specific primary antibodies. Protein expression was detected using species-specific HRP/DAB (ABC) detection IHC kit for mouse and rabbit, following the manufacturer's protocol. For negative control samples, primary antibodies were omitted from the protocol. BrdU immunohistochemical kit was used for the detection of bromodeoxyuridine.

Experiment on human samples

Chromogenic in situ hybridization (CISH)

Skin biopsies were obtained from psoriasis patients and healthy individuals who underwent plastic surgery, following the principles of the Helsinki Declaration, by the physicians of the Department of Dermatology at the University of Debrecen. The study was approved by the ethics committee of the University of Debrecen (registration number: 50935/2012/EKU (776/PI/2012, modified under registration number V/2072-2 /2020/EKU). Individuals providing the samples were adequately informed in advance and gave consent for the publication of images made from their skin samples. In the clinical skin samples, we examined the expression of PARP2 mRNA. The samples were obtained from the symptomatic scalp of 5 psoriasis patients and the normal scalp of 4 healthy individuals. In order to detect PARP2 mRNA in the sections, we applied in situ hybridization. CISH was performed on 5 µm thick sections of formalin-fixed paraffin-embedded (FFPE) samples. We used 100 nM double-digoxigenin-labeled PARP2-specific or a non-specific mRNA negative control probe containing locked nucleic acid (LNA) as per the manufacturer's instructions. The sections were treated with 2x proteinase K solution for 15 minutes, followed by the application of 100 nM pre-linearized (at 90 °C for 4 minutes) probe mixture diluted in 1x ISH buffer. Hybridization was carried out at 53 °C for PARP2-specific and 57 °C for the negative control LNA probe for 60 minutes. For visualization, alkaline phosphatase-conjugated digoxigenin antibody and nitroblue tetrazolium / 5-bromo-4-chloro-indolyl-phosphate (NBT/BCIP) chromogenic substrate were applied for 2 hours at 30 °C. The slides were stained with stable liquid nuclear

red and covered with Eukitt mounting medium, followed by the placement of a coverslip. Images were captured using a Leica DM200LED microscope.

***In Silico* analysis**

During the investigation of PARP1, the RNA sequencing data from human psoriatic lesional skin were obtained from the National Center for Biotechnology Information Gene Expression Omnibus (NCBI GEO) public database (GDS5260 / ILMN_1686871 (nih.gov); GDS4602 / 208644_at (nih.gov)). For the comparison of psoriasis mouse models, we also utilized the NCBI GEO public database (GDS3907 / 1435368_a_at (nih.gov)). In the case of studying PARP2, previously published transcriptomic data from healthy skin and psoriatic lesional skin of different groups were employed, also sourced from the NCBI GEO database (<https://www.ncbi.nlm.nih.gov/geo/query/acc.cgi?acc=GSE63980>). Additionally, the RNA sequencing data obtained from IL17A+TNF α -treated sc and shPARP2 HPV-Ker cells carried out by us were used to generate heatmaps (<https://www.ncbi.nlm.nih.gov/bioproject/PRJNA889321>).

Statistical analysis

For statistical evaluation, the GraphPad Prism program was utilized. First, the distribution of the data was analyzed using the Shapiro-Wilk test. In cases of comparing two groups, an independent samples t-test was employed if the Shapiro-Wilk test indicated a normal distribution. For non-normally distributed data, the Mann-Whitney test was used. If comparisons were made among more than two groups and the distribution was normal, a one-way ANOVA test was conducted, followed by Tukey's post-hoc test. In situations where the data did not follow a normal distribution, the Kruskal-Wallis test was applied, complemented by Dunn's post-hoc test or Dunnett's post-hoc test. The intensity of immunohistochemical reactions was scored on a 0-3 scale, and a chi-square test (χ^2) was used for statistical analysis between groups.

Significance values (p-values) and the number of replications (n) were presented in the figure captions.

Results

PARP1 expression is decreased in psoriasis

In the first part of our work, we aimed to explore the potential role of PARP1 in psoriasis. As a first step, our co-authors investigated IMQ-induced skin inflammation on the skin of PARP1^{+/+} and PARP1^{-/-} male mice. Previous literature data had consistently described PARP1 deletion or pharmacological inhibition as anti-inflammatory in numerous models. Thus, it was surprising to observe that the developed dermatitis was more severe in PARP1^{-/-} mice compared to PARP1^{+/+} mice (Kiss et al., 2019: **Figure 1; Figures 2A and 2B**).

We were interested in investigating how PARP1 expression changes in psoriasis. We found that the expression of PARP1 was reduced in lesional skin of psoriasis patients compared to the expression detected in normal skin samples from similar anatomical regions of healthy individuals. A similar decrease in PARP1 expression was observed when analyzing publicly available RNA sequencing data from human psoriatic lesional skin using in silico analysis from the NCBI GEO database. Immunohistochemical studies in IMQ-treated PARP1^{+/+} mouse skin also demonstrated a reduction in PARP1 expression, although not to a statistically significant extent. Conversely, when comparing psoriasis mouse models in another publicly available dataset, we observed a general decrease in PARP1 expression across these models.

All these findings suggest that the decreased expression of PARP1 in psoriasis may have a potential pathomechanical role, possibly contributing to the characteristic inflammatory processes of psoriasis, which contradicts observations in other inflammatory conditions.

Application of PARP inhibitors in combination with imiquimod enhances keratinocyte proliferation and cytokine production

Aberrant processes occurring in keratinocytes play a central role in psoriasis pathogenesis. Since our histological investigations revealed high PARP1 expression in epidermal keratinocytes, we aimed to elucidate the significance of PARP1 expression in psoriasis-like inflammatory responses using human keratinocyte cell cultures, specifically HPV-Ker cells. Depending on the cell type, PARP1 covers up to 85-90% of measurable PARP activity in cells; therefore, in our cell culture experiments, we employed PARP inhibitors (olaparib, rucaparib, and PJ34) to block PARP1. One of the most reliable methods for monitoring PARP activity in cells is the detection of ADP-ribose polymers with PAR-specific antibodies. As shown in the representative Western blot, treating HPV-Ker keratinocytes with

IMQ increased the level of PARylation compared to vehicle-treated control cells. Furthermore, all three PARP inhibitors used effectively reduced PARylation in the cells. Using SRB staining, we observed that, within the concentration and duration we employed, IMQ alone did not impact cell proliferation. However, PARP inhibitors significantly enhanced keratinocyte proliferation compared to IMQ, and this effect was even more pronounced when PARP inhibitors were used in combination with IMQ.

Additionally, we examined the changes in expression of some cytokines relevant to psoriasis in HPV-Ker cells following IMQ treatment and PARP inhibition. Under IMQ treatment, the mRNA expression of IL1 β , IL6, IL8, and IL23A significantly increased in keratinocytes. Moreover, when IMQ was combined with PARP inhibitors, cytokine expression further escalated in the cells, particularly notable for IL6 and IL8. These data were consistent with our *in vivo* observations.

The effect of PARP1 on keratinocyte proliferation depends on TRPV1 activity

Transient receptor potential vanilloid (TRPV)1, a non-selective cation channel, has been identified as a positive mediator of several factors involved in psoriasis pathogenesis. Therefore, we examined whether suspending the detrimental effects of PARP inhibition during IMQ treatment could be achieved by inhibiting TRPV1. In SRB assays, we found that pre-treatment of HPV-Ker cells with the TRPV1-specific inhibitor AMG9810 prevented the increase in total protein content and proliferation of cells previously observed with the combined application of IMQ and PARP inhibitors. TRPV1 is phosphorylated by cAMP-dependent protein kinases, including protein kinase C (PKC), which sensitizes its activity. PKC also regulates PARP1 activity, so we investigated whether the PKC inhibitor Gö6976 influenced the effects of IMQ and PARP inhibition on keratinocyte proliferation, but no change was observed in this case.

PARP2 Expression Increases in the Skin of Psoriasis Patients

In light of the results presented earlier, we were curious to determine whether PARP2, the "sibling" of PARP1, might play a role in psoriasis.

As a first step, we examined the expression of PARP2 in the lesional skin of psoriasis patients and normal skin samples from similar regions of healthy individuals using chromogenic *in situ* hybridization (CISH) method. In normal skin, we observed low-level expression of

PARP2 mRNA, while in psoriatic epidermis, there was a significant increase in PARP2 mRNA expression.

Deletion of PARP2 reduces the severity of IMQ-induced psoriasis-like dermatitis in mice

In order to characterize the significance of PARP2 expression in psoriasis, we reapplied the well-known psoriasis mouse model induced by IMQ on PARP2^{-/-} and PARP2^{+/+} male mice. By the fifth day of the experiment, it was clearly evident that the developed lesions were less severe in IMQ-treated PARP2^{-/-} (PP) mice compared to wild-type (WP) mice treated with IMQ. Hematoxylin and eosin (H&E) staining of lesion sections revealed typical features of IMQ-induced dermatitis in the lesional skin of WP mice, such as increased keratinocyte proliferation in the basal layer, dilated capillaries, and dermal cellular infiltration. However, these alterations were considerably less pronounced in the sections of PP mice. Epidermal thickening was more prominent in the skin of WP mice compared to PP mice, as observed in comparison to vehicle-treated wild-type (WC) and PARP2^{-/-} (PC) mice. PP mice showed significantly fewer BrdU-positive nucleas in their epidermis compared to WP mice, indicating a lower proliferation rate of PARP2^{-/-} keratinocytes.

PP mice exhibited milder inflammation in their skin, indicated by lower levels of IL17A and TNF α in the lesional skin lysates of PP mice compared to WP mice. Immunohistochemical (IHC) analyses of the lesion sections showed that involucrin, a marker of early differentiation, retained its distinctive expression in the stratum spinosum of PP mice, while in the WP group, involucrin expression extended throughout the entire epidermis. Additionally, the late terminal differentiation marker keratin 10 exhibited significantly higher expression in the epidermis of PP mice compared to WP mice.

Overall, these data point to the role of PARP2 in keratinocyte activation associated with psoriasis-related inflammation.

PARP2-depleted human keratinocytes retain terminal differentiation after treatment with psoriasis-specific cytokines

To characterize the role of PARP2 in keratinocytes, we silenced PARP2 in HPV-Ker human keratinocytes using a lentiviral vector containing PARP2-specific shRNA, resulting in approximately 70% reduction in PARP2 protein expression in shP2 HPV-Ker cells compared to control cells carrying a negative control sequence (sc cells). The sc and shP2 HPV-Ker cells were stimulated with IL17A and TNF α combination, as previously described that the synergistic

effect of IL17A and TNF α induces transcriptomic changes in keratinocytes that correlate significantly with genomic changes characteristic of psoriasis. Upon IL17A and TNF α treatment, PARP2 expression in keratinocytes increased. In the presence of IL17A and TNF α during differentiation, the expression of CK10 was significantly higher in shP2 keratinocytes compared to sc keratinocytes. Cell cycle analysis revealed an increase in the proportion of S-phase cells in sc HPV-Ker cells upon IL17A + TNF α treatment, but this was not characteristic in shP2 cells.

The findings in human keratinocytes appear to align with those observed in the skin of psoriasis patients and the IMQ-induced mouse model of psoriasis in terms of PARP2 function. This prompted us to further investigate the role of PARP2 in inflammatory regulation.

The activation of NF- κ B mediated by pro-inflammatory cytokines is inhibited in PARP2-silenced keratinocytes

To understand mechanisms regulated by PARP2 in keratinocytes, we conducted comprehensive transcriptome analyses using RNA sequencing in both sc and shP2 HPV-Ker cells treated with either vehicle or IL17A+TNF α . We identified over 300 dysregulated genes between vehicle-treated sc and shP2 keratinocytes. When comparing vehicle-treated and IL17A+TNF α -treated sc HPV-Ker cells, we found differential expression in 64 genes, whereas in the comparison of vehicle or IL17A+TNF α -treated shP2 cells, there were only 20 genes showing differential expression. This indicates suppression of IL17A and TNF α -induced pathways in PARP2-silenced keratinocytes. TNF α alone or in combination with IL17A primarily acts through NF- κ B activation, a critical pro-inflammatory pathway in psoriasis development. Indeed, during an in silico analysis of previously published RNA sequencing data from 92 psoriatic and 82 normal skin samples, we found increased expression of several NF- κ B target genes, including CXCL8 (IL8), CXCL1, IL23A, IL6, and colony-stimulating factor (CSF)2 in psoriatic skin. In our RNA sequencing data, IL17A+TNF α treatment led to even greater induction of these genes' expression in sc HPV-Ker cells, while this induction was considerably smaller in shP2 cells.

Subsequently, we examined the phosphorylation of the NF- κ B p65 subunit, an indicator of NF- κ B activation, in the cell's nuclear fraction. Upon IL17A and TNF α treatment, p65 phosphorylation indeed increased in sc cells but not in shP2 cells.

Among the NF- κ B target genes, we chose two markers for further investigation, IL6 and IL23A, both associated with psoriasis-related inflammation in both human and mouse models.

First, through RT-qPCR measurements, we validated the RNA sequencing data, confirming that IL6 and IL23A mRNA expression was significantly less elevated in shP2 keratinocytes compared to sc keratinocytes in response to IL17A and TNF α . Additionally, the increased IL6 secretion and IL23A protein expression induced by IL17A+TNF α were lower in shP2 keratinocytes compared to sc cells.

These data suggest that PARP2 influences NF- κ B activity and thereby mediates NF- κ B-associated inflammatory pathways.

Increased estradiol production inhibits NF- κ B in PARP2-depleted keratinocytes

During the analysis of the dataset derived from RNA sequencing, we found markers of steroidogenesis (such as the cholesterol transporter StarD5) that exhibited high induction in shP2 HPV-Ker cells compared to sc cells, in line with our previous studies associating PARP2 with cholesterol and steroid homeostasis regulation. Additionally, the expression of 17 β -hydroxysteroid dehydrogenase-3 (HSD17B3), which catalyzes the conversion of androstenedione to testosterone, was increased in shP2 cells. Moreover, the expression of CYP19A1, encoding aromatase, which converts testosterone to estrogen, and G-protein-coupled estrogen receptor 1 (GPER1) was induced in shP2 cells, suggesting an enhanced estrogen response in PARP2-silenced keratinocytes. These gene expression changes piqued our interest, as both estradiol (E2), the primary human estrogen, and GPER1 are capable of inhibiting NF- κ B activation in various tissues. Therefore, our hypothesis was that the inhibition of NF- κ B activation could be a consequence of enhanced estrogen action in shP2 cells.

Firstly, we confirmed the induction of aromatase expression in PARP2-silenced keratinocytes. In line with this, significantly higher estradiol concentrations were detected in the supernatant of shP2 HPV-Ker cells compared to sc HPV-Ker cells. We then investigated whether PARP2 enzymatic activity might play a role in regulating estradiol production. To this end, we inhibited PARP2 using a specific inhibitor, UPF1069, which led to a robust increase in estradiol secretion from HPV-Ker cells. Furthermore, treatment with talazoparib, a potent inhibitor of both PARP1 and PARP2, at a higher concentration, resulted in a smaller yet significant increase in estradiol production in HPV-Ker cells compared to UPF1069. These data suggest that PARP2 enzymatic activity, although not fully understood, participates in the regulation of aromatase activity and thus estradiol synthesis in keratinocytes.

When HPV-Ker cells were maintained in estradiol-containing medium before IL17A and TNF α stimulation, lower IL6 mRNA expression and secretion were observed after

treatment compared to estradiol absence, indicating that estradiol could indeed exert anti-inflammatory effects against the response triggered by IL17A+TNF α in keratinocytes.

Next, using immunofluorescence, we examined the presence of I κ B α in the cytoplasm of keratinocytes, which anchors NF- κ B in the cytoplasm, preventing its nuclear translocation and the transcription of NF- κ B target genes. Upon IL17A+TNF α treatment, I κ B α degradation was observed in sc HPV-Ker cells, whereas this effect was less pronounced in shP2 cells. However, when sc HPV-Ker cells were pretreated with estradiol before cytokine stimulation, I κ B α degradation occurred to a lesser extent, corroborating earlier results indicating estradiol-mediated inhibition of I κ B α degradation.

To functionally link the protective effect exerted by estradiol to the impact of PARP2 silencing, we inhibited estradiol synthesis in HPV-Ker cells using the aromatase inhibitor exemestane (EXE). We found that the activation of NF- κ B p65 subunit in response to IL17A and TNF α increased in shP2 cells upon exemestane pretreatment, reaching levels similar to those observed in sc cells. Consistently, exemestane application reduced the originally observed difference in IL6 secretion and IL23A protein expression between sc and shP2 HPV-Ker cells following IL17A+TNF α treatment.

It seems, therefore, that the inhibition of estradiol synthesis unleashed the NF- κ B activation inhibition mediated by PARP2 depletion in keratinocytes, suggesting that the anti-inflammatory effect of PARP2 silencing in keratinocytes is indeed a consequence of increased estradiol production.

Aromatase function is necessary for the anti-inflammatory effect mediated by PARP2 in mouse skin

We investigated how inhibition of skin aromatase activity influences IMQ-induced skin inflammation in our mice. Separate groups of PARP2 $^{+/+}$ and PARP2 $^{-/-}$ mice were treated with solvent (ethanol) or IMQ (WP and PP mice). Additionally, we formed new groups of PARP2 $^{+/+}$ and PARP2 $^{-/-}$ mice that received epicutaneous exemestane treatment prior to IMQ treatment (WPE and PPE mice).

Exemestane treatment increased the cumulative visual score of IMQ-induced lesions in both PARP2 $^{+/+}$ and PARP2 $^{-/-}$ mice, indicating a protective role of aromatase activity in the skin. Exemestane nullified the anti-inflammatory effect of PARP2 deletion in the IMQ model, as evidenced by the increase in relevant cytokine levels measured from the mice skin lysates, comparing PPE mice to PP mice. IL17C, a central pro-inflammatory cytokine in psoriatic

inflammation, was quantified from the skin lysates through a separate ELISA measurement, and similar to the cytokine array results, a significant increase was observed due to exemestane treatment.

Immunohistochemical analyses were conducted on sections from the mice's lesioned skin. In line with our findings in human keratinocytes, epidermal keratinocytes of PARP2^{-/-} mice exhibited higher aromatase expression compared to PARP2^{+/+} mice, regardless of the treatment applied (PP and PPE mice vs. WP and WPE mice). Similarly, aligning with the in vitro data, significantly more phospho-p65-positive nuclei were found in the epidermis of WP mice than in PP mice. However, aromatase inhibition also led to a significant increase in p65 phosphorylation in the skin of PPE mice compared to PP mice, thereby eliminating the originally observed difference in p65 activation between the PARP2 knockout and wild-type mouse groups. Additionally, aromatase inhibition negatively impacted keratinocyte differentiation, as evidenced by decreased K10 expression in the epidermis of exemestane-treated mice compared to those treated only with IMQ.

In summary, these results suggest that the protected phenotype observed in PARP2^{-/-} mice against the severity of IMQ-induced dermatitis in the skin is partially developed due to increased aromatase activity, at least in part.

Aromatase expression decreases in human psoriatic lesions

Finally, we examined aromatase expression in human skin using the same psoriatic and healthy samples in which we previously analyzed PARP2 expression. In healthy samples, we found high aromatase expression, evenly distributed throughout the layers of the epidermis. In contrast, in psoriatic epidermis, aromatase expression showed an overall decrease, mainly limited to the stratum granulosum. This suggests that skin estrogen biosynthesis is suppressed in psoriasis. This observation, coupled with the above results, indicates a potential correlation between PARP2 expression and estrogen synthesis in epidermal keratinocytes, which could contribute to the regulation of local inflammatory processes in the pathogenesis of psoriasis.

Discussion

PARP1 and PARP2 belongs to the family of enzymes catalyzing ADP-ribosylation, a type of post-translational protein modification. Their catalytic function is primarily activated in response to DNA damage, and as a result, PARP1 and PARP2 were long known for their crucial role in DNA damage repair.

As the number of studies related to PARP1 increased, researchers recognized that PARP1 also participates in the regulation of numerous inflammatory processes. PARP1 acts as a positive modulator of several pro-inflammatory transcription factors (e.g., NF-κB) and appears to mainly contribute to the development of Th2-type inflammation. Consequently, genetic deletion or pharmacological inhibition of PARP1 led to anti-inflammatory effects in experimental models of various Th2-type inflammatory conditions.

Studies regarding PARP2 are relatively limited in comparison to PARP1 in the literature. However, based on research conducted over the past decade, it has become increasingly evident that PARP2 plays unique roles in regulating a diverse range of physiological processes, including transcription, cell differentiation, mitochondrial biogenesis, lipid and steroid biosynthesis, and metabolic homeostasis in various cells and tissues. Nevertheless, there is limited data available about the role of PARP2 in inflammatory processes, but current information suggests that, unlike PARP1, PARP2 might not participate in the regulation of Th2-type inflammation.

Psoriasis is one of the most common chronic inflammatory skin diseases, characterized by the formation of distinctive plaques on the skin due to hyperproliferation and abnormal differentiation of epidermal keratinocytes. The currently accepted explanation attributes the development of psoriasis to certain populations of T cells, primarily Th17 cells, and highlights the central role of the IL23/IL17 cytokine axis in mediating the inflammation characteristic of psoriasis. However, the pathomechanism of psoriasis is a complex process in which the role of T cells is not exclusive; epidermal keratinocytes likely have an important role in the appearance of the disease. They may contribute to the initiation, maintenance, and amplification of inflammation by secreting molecules involved in recruiting, retaining, and activating T cells.

The main objective of this study was to characterize the roles of PARP1 and PARP2 in a Th17-type inflammatory process, specifically in psoriasis, with a particular focus on processes regulated in keratinocytes.

Inhibition of PARP1 enhances imiquimod-induced processes in keratinocyte cells

Our experiments were prompted by studies characterizing the role of PARP1 in Th2-type inflammation, while its potential role in Th17-mediated inflammation remains poorly characterized. Thus, we investigated the effects of inhibiting PARP1 in processes characteristic of psoriasis in keratinocytes.

Our findings contradicted previous knowledge about the role of PARP1 in inflammation. We observed that genetic deletion of PARP1 exacerbated the symptoms in a mouse model of imiquimod-induced psoriasis, suggesting a possible role of PARP1 in the development of psoriatic inflammation. To understand the underlying processes, we first conducted histological studies and found that PARP1 expression decreased in the lesional epidermis of psoriasis patients compared to normal skin, corroborating the observations from our mouse model and reinforcing the notion that the absence of PARP1 might contribute to the onset of psoriatic inflammation.

Subsequently, in *in vitro* human keratinocyte cell cultures (HPV-Ker cells), we demonstrated that combining PARP1 inhibition with IMQ treatment recapitulated the *in vivo* mouse model results. Specifically, PARP inhibitors amplified the effects of IMQ on keratinocyte proliferation and further enhanced the induction of pro-inflammatory cytokines (IL6, IL1 β , IL8, IL17, and IL23A).

We found that pharmacological blockade of the non-selective cation channel TRPV1 was able to suspend the proliferative effects of PARP inhibitors in HPV-Ker keratinocytes. TRPV1 is relatively highly expressed in skin tissue, not only in keratinocytes but also in peripheral sensory nerve fibers and resident immune cells. TRPV1 can be activated by exogenous and endogenous inflammatory mediators, triggering the secretion of TRPV1 neuropeptides and inducing a neurogenic inflammatory response. Previous studies have associated TRPV1 with chronic inflammatory skin conditions, including the pathomechanism of psoriasis. Interestingly, the modulatory effects of TRPV1 in the IMQ-induced psoriasis model have also been described. Moreover, an antagonistic interaction between TRPA1 and TRPV1 has been suggested in the IMQ model. Similarly, we propose a potential antagonistic relationship between PARP1 and TRPV1, although the characterization of this interaction requires further investigation. PKC, a characteristic modulator of TRPV1, also influences PARP1 activity. Therefore, we explored the possibility that PKC activity might also contribute to this potential functional interaction between PARP1 and TRPV1. However, the application of a PKC inhibitor did not affect the proliferative effects of PARP inhibitors in our model.

In conclusion, our results suggest that PARP1 may play a contrasting role in Th17-type inflammation, such as in psoriasis, compared to Th2-mediated processes. We recommend a deeper investigation of this mechanism in future research endeavors.

PARP2 contributes to inflammation development in psoriasis through modulation of keratinocyte estradiol biosynthesis

PARP2 is the second-largest contributor to PARP activity in cells, following PARP1. Given our previous findings suggesting a potential role for PARP1 in psoriasis, our research aimed to investigate whether PARP2 might also play a role in psoriasis.

We observed elevated expression of PARP2 in the lesional skin of psoriasis patients. Contrary to the severity of imiquimod (IMQ)-induced dermatitis observed in PARP1^{-/-} mice, PARP2^{-/-} mice exhibited milder symptoms compared to wild-type mice. This suggests that PARP1 and PARP2 are involved in distinct mechanisms regulating psoriatic inflammation. Notably, the IMQ-induced psoriasis model isn't the first Th17-mediated process in which PARP1^{-/-} and PARP2^{-/-} mice displayed contrasting phenotypes. In experimental autoimmune encephalomyelitis (EAE), a mouse model of multiple sclerosis, PARP1 deletion worsened the condition, while PARP2 deletion mitigated the characteristic neurological inflammation. However, the underlying processes require further elucidation.

Uniquely, PARP2 has been linked to various aspects of cholesterol and steroid synthesis, particularly in tissues with intensive lipid metabolism. In the skeletal muscles of PARP2^{-/-} mice, elevated expression of 17 β -dehydrogenase-11 (HSD17B11), an enzyme involved in androsterone biosynthesis, and 5 α -reductases (SRD5A1, 2), which catalyze the transformation of testosterone into the even stronger androgen dihydrotestosterone (DHT), was observed. Consequently, DHT levels increased in the skeletal muscles of PARP2^{-/-} mice, without affecting systemic DHT levels. Additionally, PARP2 is involved in the androgen receptor signaling pathway in the prostate. Our results demonstrate that the protective effect resulting from PARP2 genetic deletion or depletion against psoriasis-like inflammation depends on keratinocyte aromatase function and estradiol biosynthesis, as well as estradiol-mediated inhibition of NF- κ B activation.

Although the therapeutic potential of estrogens in psoriasis has been considered, long-term systemic estrogen therapy can carry adverse effects, and systemic estrogen treatment hasn't been attempted in psoriasis. Based on our findings, we suggest enhancing keratinocyte's own

estrogen biosynthesis through PARP2 inhibition as a potential novel approach to psoriasis therapy.

Estrogens have a complex role in immunomodulation. While psoriasis generally improves during pregnancy and worsens during menopause, some patients experience aggravated symptoms during pregnancy. Estrogen's positive impact on psoriasis could be explained by its ability to shift the balance from Th1/Th17-type immunity towards Th2-mediated immunity. However, estrogen receptor (ER) activity significantly depends on estrogen dosage and the model system under study, meaning ER activation could either increase or decrease pro-inflammatory cytokine production depending on the applied estrogen concentration. One study indicates that a minimal estradiol concentration of around 10^{-10} M is required for effective NF- κ B inhibition and subsequent anti-inflammatory effects, an approximate concentration we observed in our HPV-Ker cell models with silenced or inhibited PARP2. In the context of our study, we assume that during psoriasis progression, Th1 and Th17-derived cytokines (such as TNF α and IL17A) may induce PARP2 in keratinocytes. This may then inhibit aromatase activity and estradiol synthesis, contributing to NF- κ B activation. However, the detailed mechanics of such a regulatory cascade need further investigation.

Current successful therapies for psoriasis involve biological agents targeting IL17A or TNF α . However, these therapies come with risks, driving the need for better-tolerated options. Several PARP inhibitors are used clinically, particularly for systemic application in certain cancer therapies. These include FDA-approved veliparib, rucaparib, olaparib, niraparib, talazoparib, as well as Chinese NMPA-approved fluzoparib and pamibarib. These pan-PARP inhibitors target both PARP1 and PARP2, and possibly other PARP isoforms. Therefore, selective targeting of PARP2 isn't currently feasible with existing PARP inhibitors. Nevertheless, our results demonstrate that the pan-PARP inhibitor talazoparib can enhance keratinocyte estradiol production similarly to PARP2 silencing or specific inhibition with UPF1069. Considering the likely consequence of PARP2 deficiency—increased keratinocyte estradiol synthesis—our findings suggest the potential use of PARP inhibitors in psoriasis treatment. However, the applicability of PARP inhibitors in this context must be further studied and evaluated.

In summary, we have identified an unknown mechanism by which PARP2 can contribute to the regulation of inflammatory processes and have identified a potential therapeutic target for psoriasis. Our study could contribute to the development of PARP2-specific inhibitors, and we recommend further research to clarify the precise role of PARP2 in inflammation and immune regulation.

Summary

As members of the poly(ADP-ribose) polymerase enzyme family, PARP1 and PARP2 are primarily responsible for the majority of cellular PARP activity, and their activity was first described during DNA damage repair. However, research over the past decades has revealed diverse biological functions of PARP1 and PARP2, including roles in cell death, cell differentiation, lipid homeostasis, cellular energetics, and inflammation regulation. PARP activation has been described in numerous Th2-mediated inflammatory processes, but investigations have mainly focused on the role of PARP1, with limited information about the role of PARP2 in inflammation. In our work, we examined the roles of PARP1 and PARP2 in a Th17-mediated inflammatory skin disease, psoriasis.

Firstly, with the help of our co-authors, we found that contrary to our current knowledge, PARP1 could unexpectedly act as an anti-inflammatory factor in psoriasis, as genetic deletion of PARP1 worsened symptoms in a mouse model of imiquimod-induced psoriasis. In human samples, we demonstrated that PARP1 expression decreases in psoriatic lesions compared to skin samples from control individuals. In HPV-Ker keratinocytes treated with imiquimod, PARP inhibition increased keratinocyte proliferation and induced the expression of certain pro-inflammatory cytokines in line with *in vivo* results. Furthermore, we showed that the former effects of PARP inhibition in keratinocytes were dependent on TRPV1 activity. Based on these findings, we can conclude that the role of PARP1 in regulating Th17 type inflammation might differ from what we observed in Th2 type processes.

In contrast, we observed an increase in PARP2 mRNA expression in lesional skin of psoriasis patients and the deletion of PARP2 attenuated the imiquimod-induced psoriasis-like dermatitis in mice. Silencing PARP2 in human keratinocytes prevented the increased proliferation, maintained their terminal differentiation, and reduced the production of inflammatory mediators following treatment with IL17A and TNF α . Behind these observations, we found that aromatase expression was induced in PARP2 $^{-/-}$ mouse epidermis and PARP2 deficient human keratinocytes, leading to elevated estradiol production that inhibited NF- κ B activation and thereby inflammation in keratinocytes. Steroidogenic changes have been described in psoriasis before, and our observations complement these findings by demonstrating a decrease in aromatase expression in psoriatic lesions.

In summary, our data identify PARP2 as a modulator of estrogen biosynthesis in epidermal keratinocytes, that may be relevant in Th17 type inflammation.



Registry number: DEENK/365/2023.PL
Subject: PhD Publication List

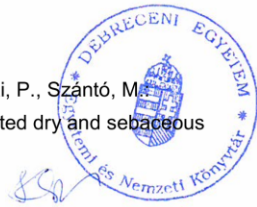
Candidate: Dóra Antal
Doctoral School: Doctoral School of Molecular Medicine
MTMT ID: 10071151

List of publications related to the dissertation

1. **Antal, D.**, Pór, Á., Kovács, I., Dull, K., Póloska, S., Ujlaki, G., Demény, M. Á., Szöllősi, A. G., Kiss, B., Szegedi, A., Bai, P., Szántó, M.: PARP2 promotes inflammation in psoriasis by modulating estradiol biosynthesis in keratinocytes. *J. Mol. Med. (Berl)*. 101 (8), 987-999, 2023.
DOI: <http://dx.doi.org/10.1007/s00109-023-02338-z>
IF: 4.7 (2022)
2. Kiss, B. K., Szántó, M., Hegedűs, C., **Antal, D.**, Szödényi, A., Márton, J., Méhes, G., Virág, L., Szegedi, A., Bai, P.: Poly(ADP-ribose) polymerase-1 depletion enhances the severity of inflammation in an imiquimod-induced model of psoriasis. *Exp. Dermatol.* 29 (1), 79-85, 2020.
DOI: <https://doi.org/10.1111/exd.14061>
IF: 3.96

List of other publications

3. **Antal, D.**, Alimohammadi, S., Bai, P., Szöllősi, A. G., Szántó, M.: Antigen-Presenting Cells in Psoriasis. *Life (Basel)*. 12 (2), 1-10, 2022.
DOI: <http://dx.doi.org/10.3390/life12020234>
IF: 3.2
4. **Antal, D.**, Janka, E. A., Szabó, J., Szabó, I. L., Szegedi, A., Gáspár, K., Bai, P., Szántó, M.: Culture-based analyses of skin bacteria in lesional moist, and unaffected dry and sebaceous skin regions of hidradenitis suppurativa patients. *J. Eur. Acad. Dermatol. Venereol.* 36 (9), e731-e733, 2022.
DOI: <http://dx.doi.org/10.1111/jdv.18254>
IF: 9.2





UNIVERSITY of
DEBRECEN

UNIVERSITY AND NATIONAL LIBRARY
UNIVERSITY OF DEBRECEN
H-4002 Egyetem tér 1, Debrecen
Phone: +3652/410-443, email: publikaciok@lib.unideb.hu

5. Szántó, M., Dózsa, A., **Antal, D.**, Szabó, K., Kemény, L. V., Bai, P.: Targeting the gut-skin axis -
Probiotics as new tools for skin disorder management?
Exp. Dermatol. 28 (11), 1210-1218, 2019.
DOI: <http://dx.doi.org/10.1111/exd.14016>
IF: 3.368

Total IF of journals (all publications): 24,428

Total IF of journals (publications related to the dissertation): 8,66

The Candidate's publication data submitted to the iDEa Tudóstér have been validated by DEENK on
the basis of the Journal Citation Report (Impact Factor) database.

31 July, 2023

